Applied Physics Letters ARTICLE pubs.aip.org/aip/apl

Parallel 2DHG conduction in AlN/GaN/AlN HEMTs: Leakage mechanisms and electric field distribution

Cite as: Appl. Phys. Lett. **128**, 033504 (2026); doi: 10.1063/5.0310993
Submitted: 6 November 2025 · Accepted: 25 December 2025 ·
Published Online: 20 January 2026

Yuke Cao,[1,a] James W. Pomeroy,[1] Austin Hickman,[2] Reet Chaudhuri,[2] Debdeep Jena,[2] Huili Grace Xing,[2] and Martin Kuball[1]

AFFILIATIONS

[1]Centre for Device Thermography and Reliability, H.H. Wills Physics Laboratory, University of Bristol, Tyndall Avenue, Bristol BS8 1TL, United Kingdom

[2]School of Electrical and Computer Engineering, Department of Material Science and Engineering, Kavli Institute, Cornell University, Ithaca, New York 14853 USA

[a)]Author to whom correspondence should be addressed: yuke.cao@bristol.ac.uk

ABSTRACT

We provide direct evidence of two-dimensional hole gas (2DHG) conduction occurring in parallel with the two-dimensional electron gas (2DEG) channel in AlN/GaN/AlN high-electron-mobility transistors, using combined electrical characterization and electric-field-induced second harmonic generation. Anomalous OFF-state leakage and diode-like field distributions, which are also confirmed in isolation structures where the top heterostructures along with the 2DEG channel have been etched, reveal a buried leakage path mediated by the 2DHG. This leakage arises from Fowler–Nordheim tunneling with electron–hole pairs generation under the gate, which activates a vertical 2DEG–2DHG diode-like pathway, and from Poole–Frenkel transport that connects the 2DHG to the ohmic contacts. An equivalent circuit model is proposed to describe these mechanisms. The upper bound of the buried 2DHG sheet resistance is estimated to be 10 MΩ/sq, while the vertical resistance between the 2DHG and n^{++}GaN is 35 MΩ mm. These findings provide a direct visualization and a comprehensive model of 2DHG-mediated leakage, offering design strategies to suppress parasitic conduction and improve device performance.

Gallium nitride (GaN)-based high electron mobility transistors (HEMTs) have been the leading high-efficiency microwave power amplifiers (PAs) operating in the 3–30 GHz range.[1] However, RF power in conventional AlGaN/GaN at higher frequencies is limited by carrier confinement (short channel effects) and thermal management. Recently, the AlN/GaN/AlN platform has emerged as a promising alternative for mm-wave devices.[2,3] AlN's ultrawide bandgap (6.2 eV) provides improved two-dimensional electron gas (2DEG) channel confinement and higher thermal conductivity (340 W/mK) compared with GaN, enabling aggressive device scaling and superior power handling. This structure also enables the p-channel field effect transistors (p-FETs) using the polarization-induced 2D hole gas (2DHG) at the bottom GaN/AlN interface.[4] The coexistence of 2DEG and 2DHG represents a significant step toward an energy-efficient all-nitride complementary architecture,[5] though it can also cause device challenges.

A critical consideration in this 2DEG-2DHG bilayer structure is its potential impact on device operation. The 2DEG and 2DHG layers may function as parallel conduction paths when contacted simultaneously, such as using soldered indium contacts.[6] For high-performance scaled devices, regrown ohmic contacts are typically optimized to access only one carrier type. Consequently, recent research has primarily focused on their indirect electrical effects, such as carrier mobility influenced by internal electric fields.[7,8] Nonetheless, signs of parallel conduction have been observed, including diode-like behavior in AlN/GaN/AlN structures,[6] elevated-temperature RF loss in GaN/AlInGaN/GaN structures,[9] and transconductance overshoot in AlGaN/GaN/AlN/structures.[10] These observations suggest that the buried 2DHG may form a leakage path, particularly in the OFF state, yet its role remains unresolved.

In this work, we combine electrical characterization with electric-field-induced second harmonic generation (EFISHG) to directly probe leakage and electric field distribution in AlN/GaN/AlN HEMTs. We demonstrate that the 2DHG forms a parallel conduction path through gate-assisted carrier injection and Poole–Frenkel vertical leakage. This study provides direct evidence of 2DHG-mediated leakage in thick-channel AlN/GaN/AlN HEMTs and outlines strategies to suppress parasitic conduction.

Figure 1(a) illustrates the AlN/GaN/AlN HEMT structure investigated. The epitaxial stack, grown on a 6H-silicon carbide (SiC) substrate,

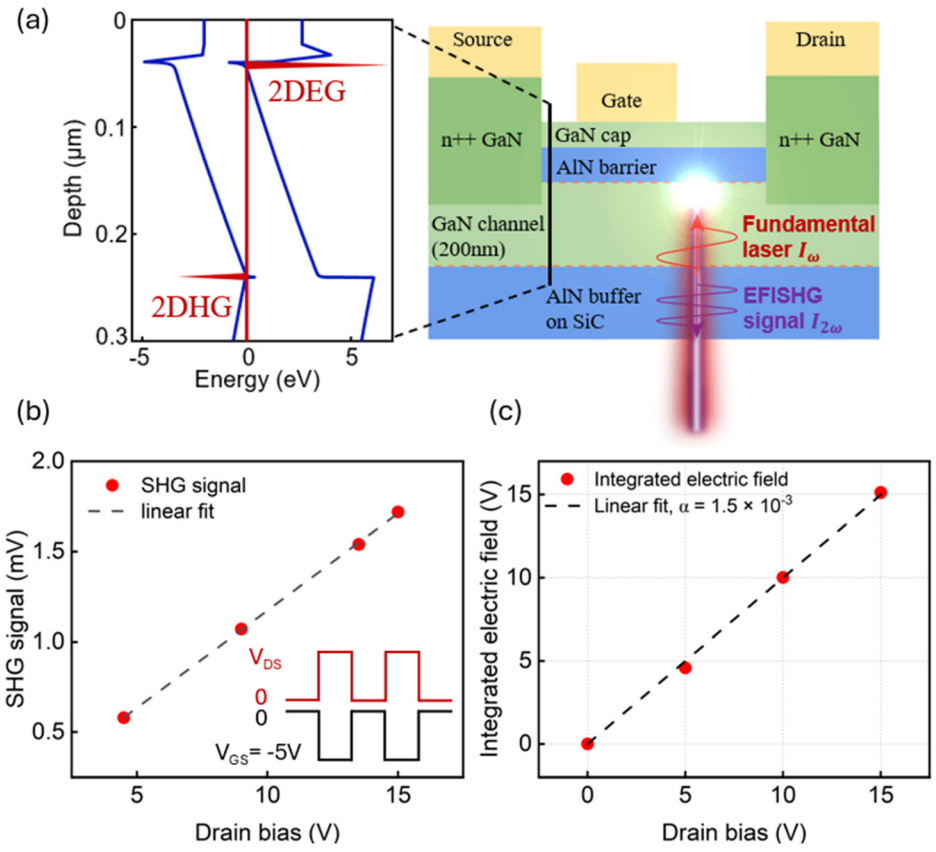

FIG. 1. (a) Schematic of the AlN/GaN/AlN HEMTs, showing the device structure, the EFISHG measurement, and the band diagram. (b) SHG signal at the drain-side gate edge as a function of drain bias. Inset: Bias modulation waveform on drain and gate during the EFISHG measurement. (c) Integrated electric field induced by the drain bias between the source and the drain.

comprises a 2 nm GaN cap layer, 5 nm AlN barrier, 200 nm strain-relaxed GaN channel, and 500 nm AlN buffer. The 200 nm strain-relaxed GaN channel was designed to reduce the internal electric field and improve electron mobility.[7,11] A GaN channel up to 20 nm thick is pseudomorphically strained (~2.4%) to AlN; at 200 nm, the GaN is partially relaxed, with a measured residual strain of 0.6%. Ohmic contacts used regrown n^{++}GaN (Si-doped, $1 \times 10^{20}\,cm^{-3}$) layers, while the Schottky gate without field plates was offset toward the source. As previously reported,[12] these devices achieved state-of-the-art performance, including a record on-current of 3.6 A/mm and maximum oscillation frequency (f_{max}) of 233 GHz. The simulated band diagram in Fig. 1(a) indicates the formation of 2DEG at the upper AlN/GaN interface and 2DHG at the lower GaN/AlN interface, assuming no other charged defects are present.

EFISHG has emerged as a powerful technique for probing electric fields in GaN-based devices.[13–15] Figure 1(a) depicts schematically the EFISHG measurement on the AlN/GaN/AlN HEMTs. A fundamental 800 nm laser is focused onto the device channel through the transparent substrate; second harmonic generation (SHG) at 400 nm is detected via lock-in amplification. The 400 nm SHG wavelength was chosen near the GaN bandgap to enhance SHG resonantly while avoiding significant absorption; no SHG is generated in the ultra-wide bandgap AlN. The total SHG signal intensity ($I_{2\omega}$) can be expressed by[15]

$$I_{2\omega} \propto \left|E^0_{2\omega}+E^{\mathrm{EFISHG}}_{2\omega}\right|^2 \approx \left(I^0_{2\omega}+2E^0_{2\omega}E^{\mathrm{EFISHG}}_{2\omega}+\left|\chi^{(3)}I_\omega E_0\right|^2\right), \quad (1)$$

where $E^0_{2\omega}$ and $E^{\mathrm{EFISHG}}_{2\omega}$ are the intrinsic and bias-induced SHG electric fields, $E^{\mathrm{EFISHG}}_{2\omega}$ is proportional to the product of the third order susceptibility ($\chi^{(3)}$), incident laser intensity (I_ω), and electric field due to applied bias (E_0), and $I^0_{2\omega}$ is the background SHG signal intensity from $E^0_{2\omega}$.

To extract E_0 from $I_{2\omega}$, we modulate the applied voltage [inset in Fig. 1(b), 1 kHz] and thus E_0, and demodulate the SHG signal at the voltage-modulation frequency to isolate the bias-induced component ($2E^0_{2\omega}E^{\mathrm{EFISHG}}_{2\omega}+\left|\chi^{(3)}I_\omega E_0\right|^2$). The dependence of $I_{2\omega}$ on E_0 (i.e., bias) can be either quasi-linear or quadratic,[16] depending on the relative magnitudes of $E^0_{2\omega}$ and $E^{\mathrm{EFISHG}}_{2\omega}$. The linear dependence of the SHG signal at the drain-side gate edge on drain bias [Fig. 1(b)] indicates that the cross term ($2E^0_{2\omega}E^{\mathrm{EFISHG}}_{2\omega} \propto 2E^0_{2\omega}\chi^{(3)}I_\omega E_0$) in Eq. (1) dominates over the quadratic term ($\left|\chi^{(3)}I_\omega E_0\right|^2$), and $E^0_{2\omega}$ significantly surpasses the $E^{\mathrm{EFISHG}}_{2\omega}$. This large $E^0_{2\omega}$ term can effectively amplify the EFISHG signal and improve the sensitivity to electric field. Homodyne detection of E_0 is then possible via the cross term with linear dependence of $I_{2\omega}$ on E_0.

Accounting for spatially varying $E^0_{2\omega}$ and surface reflectivity (R), the electric field is extracted as

$$E_0 = \alpha\left(I_{2\omega}/\sqrt{I^0_{2\omega}\cdot \mathrm{R}}\right), \quad (2)$$

where α is an optical detection efficiency constant required for quantitative electric field determination. Practically, we first map $I^0_{2\omega}$ (at the laser-chopper frequency, no bias) and R (at the SHG wavelength),

then detect the EFISHG signal at the voltage-modulation frequency. The laser line scan is performed with a step size of 0.2 μm to obtain electric field distribution from the source to the drain contact. Notably, EFISHG is much more sensitive to lateral fields than to vertical fields,[17] typically over one order of magnitude, because the incident polarization is aligned with the source–drain direction. For the lateral field, α can be obtained by integrating the extracted lateral electric field over the channel length and equating it to the applied voltage.[13] The agreement between the drain bias and the integral of the field induced by the drain bias [Fig. 1(c)] confirms that the EFISHG signal is dominated by the lateral field between source and drain. This lateral field quantification method is applied to the transistors analyzed in the following paragraph. Beneath the source and drain contacts, no lateral field exists. A vertical-field-induced SHG signal can be observed if the vertical field is sufficiently strong.[14] This vertical field quantification is detailed in the isolation structure section.

To investigate the 2DHG at the lower GaN/AlN heterointerface, we first study an isolation structure [Fig. 2(a)] in which the 2DEG is completely removed between the n^{++} GaN contacts by mesa etching, leaving a remaining GaN channel thickness of 113 nm. This is particularly relevant for devices with thick (~200 nm) GaN channels, where reliable verification of 2DHG formation via Hall-effect measurements is hindered by the high sheet resistance arising from strain-relaxation-induced defects at the GaN/AlN heterointerface.[6] For comparison, a control sample utilizing a commercial AlGaN/GaN RF HEMT structure on SiC[13] (with an Fe-doped semi-insulating buffer and ion-implantation isolation) was employed as a baseline. Room-temperature electrical measurements [Fig. 2(b)] revealed that the source–drain leakage current was independent of contact separation. This observation effectively rules out leakage through the recessed GaN surface or the bulk as dominant contribution, as these mechanisms would typically exhibit a resistance linearly proportional to the contact separation. Instead, such behavior can arise from capacitive isolation (negligible conductive paths) or a low-resistance lateral conduction path accessed via high-resistance vertical leakage paths.[18]

To resolve this ambiguity, EFISHG was employed to probe the spatial distribution of the electric field [Fig. 2(c)]. The GaN/AlN sample exhibited vertical fields beneath both source and drain contacts, with no detectable lateral field in the channel region. This measured field is assumed to be an equivalent, uniform vertical field throughout the GaN channel layer. The parameter α in Eq. (2) is obtained by multiplying the extracted field by the channel thickness under both contacts and equating the total potential drop to the applied drain voltage. By contrast, in a control AlGaN/GaN sample[13] with similar separation-independent resistance [Fig. 2(d)], the vertical field was confined beneath the biased drain contact, while lateral field peaks were at the contact edges [Fig. 2(e)], characteristic of electrostatic fringing fields in a coplanar capacitor structure.[19] In the GaN/AlN device, the coexistence of vertical fields beneath both source and drain contacts indicates a buried conduction path accessed from both sides. The absence of a lateral field between contacts implies this buried path exhibits low resistance, effectively screening the lateral potential drop expected for a resistive surface or bulk path. The uniform vertical field extending laterally beneath source and drain contacts further demonstrates that this path not only connects the two contacts but also spreads beneath them, forming a quasi-equipotential sheet.

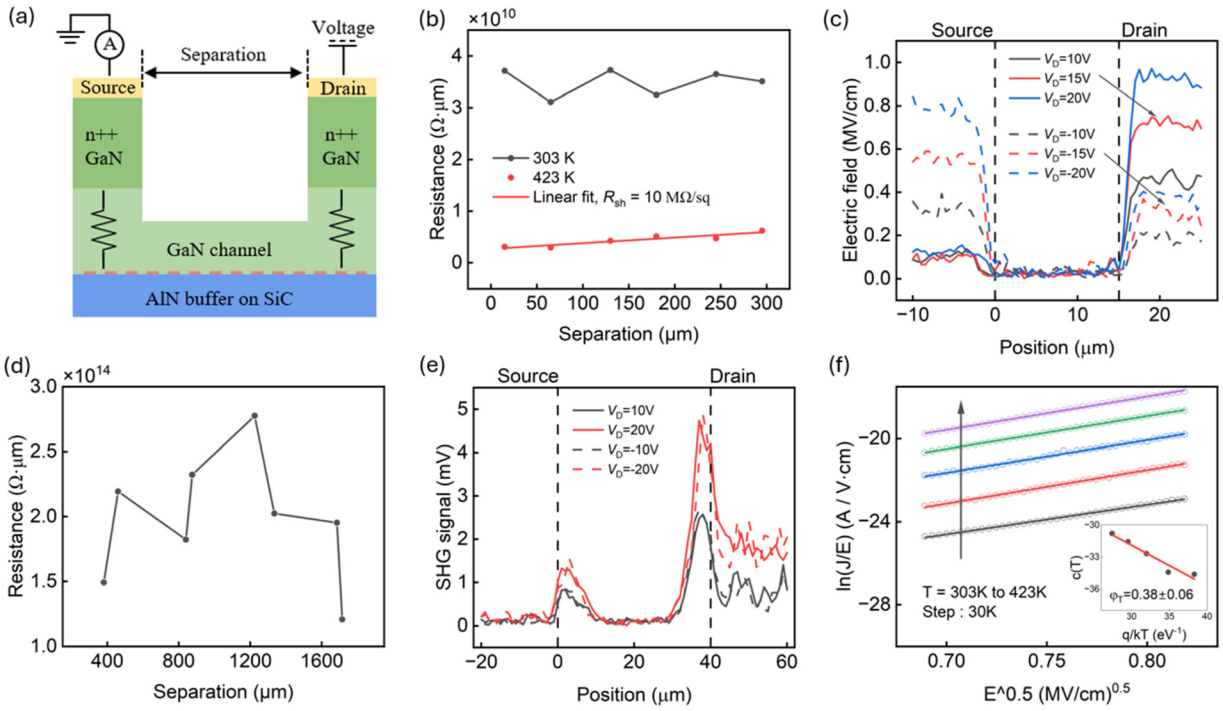

FIG. 2. (a) Schematic of the isolation structure. (b) Resistance vs source–drain separation at 20 V. (c) Electric field distribution between contacts for different bias conditions. (d) Resistance (20 V) and (e) SHG signal under different bias conditions in a conventional AlGaN/GaN HEMT isolation structure with an Fe-doped buffer layer. (f) Temperature-dependent PF plots. Inset: barrier height of 0.38 eV.

These observations collectively indicate the presence of a laterally extended, buried conductive sheet at the GaN/AlN interface, consistent with the equivalent circuit model in Fig. 2(a).

Figure 2(c) shows a symmetric spatial redistribution of the vertical electric field under the contacts, where the high-field region shifts from the drain (at $V_D > 0$) to the source (at $V_D < 0$). The observed symmetry reflects pn diode–like behavior between the n^{++} GaN and a buried p-type carrier sheet (i.e., a 2DHG). Under positive drain bias, the diode beneath the drain is reverse-biased.[20] Meanwhile, resistive coupling of the floating 2DHG to the contacts through a vertical leakage path elevates the 2DHG potential, leading to a forward-biased diode under the source. The potential distribution in these back-to-back p-n diodes thereby sustains the major voltage drop at the drain side. Reversing of the drain bias polarity shifts the reverse-biased region to the source side and thus inverts this distribution. In contrast, this polarity-dependent symmetry is absent in the control AlGaN/GaN sample, where the field remains unchanged regardless of bias polarity [Fig. 2(e)]. Due to the absence of a buried conductive channel in the control sample, the vertical field remains strictly underneath the biased drain contact regardless of polarity, never shifting to the grounded source. This, and the absence of a lateral field, provide definite evidence for a buried 2DHG electrically coupled to the contacts through vertical leakage paths in the AlN/GaN/AlN structure.

The vertical leakage path mechanism was analyzed by correlating current density (J) and vertical field (E) (supplementary material Note S1). Temperature-dependent measurements [Fig. 2(f)] revealed a linear relation between $\ln(J/E)$ and $E^{0.5}$ for different temperatures,[21] consistent with a Poole–Frenkel (PF) mechanism: field-assisted thermal emission of carriers from traps. Fitting the PF model yields a trap-related barrier height φ_T of 0.38 eV [inset of Fig. 2(f)], agreeing with prior reports[22,23] on vertical conduction in GaN HEMTs on foreign substrates with dislocation densities over $10^9\,cm^{-2}$. The threading dislocation density of the AlN/GaN/AlN HEMTs on 6H-SiC substrate in this work[6] is on the order of 10^9–$10^{10}\,cm^{-2}$. These dislocations provide abundant trap sites facilitating PF conduction.[24] This vertical PF leakage path electrically connects the buried 2DHG to the ohmic contacts originally designed for the 2DEG, thereby enabling parallel conduction in devices with the 2DEG-2DHG bilayer.

To further separate the 2DHG sheet resistance from the vertical leakage resistance (~35 MΩ mm), measurements were conducted at elevated temperatures. This approach exploits the opposite temperature dependencies of the two conduction paths: the vertical PF leakage resistance decreases with increasing temperature, while the lateral 2DHG resistance increases due to enhanced phonon scattering. At 423 K, the total resistance scales linearly with contact separation [Fig. 2(b)], from which an upper bound for the 2DHG sheet resistance is extracted as ~10 MΩ/sq. This value is three orders of magnitude higher than the room-temperature 2DHG sheet resistance of 4–20 kΩ/sq obtained in coherently strained GaN/AlN heterostructures,[6,25] which can be attributed to enhanced defect scattering and reduced polarization fields caused by partial strain relaxation in the 200-nm GaN layer. Strain relaxation leads to the formation of high density of misfit dislocations around the GaN/AlN interface,[26] which significantly degrades the mobility of 2DHG. Despite this degradation, the layer remains sufficiently conductive relative to the vertical access paths, thereby sustaining the separation-independent leakage current and the unique electric field distribution observed.

Figure 3(a) shows the three-terminal DC transfer characteristics for AlN/GaN/AlN HEMTs with 1.5 μm gate length (L_G) and 8 μm source–drain distance (L_{SD}). In conventional GaN HEMTs, OFF-state source current (I_S), gate current (I_G), and drain current (I_D) originate from combinations of source-gate (I_{SG}), drain-gate (I_{DG}), and drain–source (I_{DS}) components through the surface, barrier, or buffer [inset of Fig. 3(a)]. As gate voltage (V_G) decreases, the 2DEG channel is depleted, I_G rises, and I_S changes polarity due to the opposite signs of I_{DS} and I_{SG}.

However, in AlN/GaN/AlN HEMTs, the OFF-state current exhibits an unusual evolution. At $V_G = -5$ V [Fig. 3(b)], I_G dominates, while both I_S and I_G decrease with increasing V_D, before I_G rises again at higher V_D. For $V_D > 13.5$ V, I_D surpasses I_S and contributes more to the total gate current. In conventional AlGaN/GaN HEMTs, the reduction of I_S with V_D is usually attributed to enhanced buffer punch-through leakage I_{DS} under the depletion region.[27] In AlN/GaN/AlN HEMTs, however, this cannot account for the correlated suppression of I_G and I_S, which indicates that I_{SG} is suppressed by V_D, pointing to an additional leakage pathway.

Figure 3(c) presents the electric field distribution in the OFF-state ($V_G = -5$ V) for a device with 1.5 μm L_G and 7.5 μm L_{SD}. For clarity, the lateral field (between source and drain contacts) is quantified using α of 1.5×10^{-3}, whereas the vertical field (beneath source and drain contacts) is shown qualitatively using the same α value. Quantitative vertical field scaling requires α of 3.5×10^{-2}, which is shown in the insets. At $V_D = 0$, lateral field peaks appear at the gate edges as expected from 2DEG depletion, while a vertical field is already present beneath both source and drain contacts with only gate bias, a feature absent in conventional AlGaN/GaN HEMTs. The vertical electric fields beneath the drain (at 11 μm) and source (at −2 μm) contacts are 0.19 and 0.26 MV/cm, respectively. With increasing V_D, the drain-side vertical field strengthens, but the source-side vertical field is counterintuitively suppressed. At $V_D = 15$ V, the vertical field under the drain rises significantly to 0.59 MV/cm, while the field beneath the source drops to 0.04 MV/cm.

Figure 3(d) shows the dependence of electric field distribution on V_G at a fixed $V_D = 5$ V. Increasing V_G from −5 to −2 V reduces both lateral field peaks near the gate edges and the vertical field under the source, confirming their gate-bias origin. This gate-induced vertical field under the source contact implies a buried electrical path. Another key finding is the V_D-dependent suppression of the source-side vertical field [Fig. 3(c)], which directly correlates with the reduction in I_{SG} [Fig. 3(b)]. This correlation strongly implicates the buried 2DHG as the mediator of this previously unexplained leakage mechanism. Similar IV and electric field phenomena are consistently observed across devices with different L_G (90 nm, 1.5, 2 μm) and L_{SD} (0.6–12.5 μm), including highly scaled devices (supplementary material Fig. S1).

To investigate the leakage between the gate and the 2DHG, we analyze the gate current characteristics [Fig. 4(a)]. Three distinct regimes emerge, including moderate bias dependence for $V_G > -2$ V, strong bias-dependent leakage before threshold voltage ($V_{th} = -3.5$ V), and current saturation for $V_G < -3.5$ V. By correlating gate current density with the electric field across the barrier [Fig. 4(b) inset], the transport mechanism in each regime can be identified[28] (supplementary material Note S2). Under forward bias, the current follows thermionic emission (TE). At low reverse bias, the current significantly exceeds the TE prediction and is consistent with PF emission. Near threshold, Fowler–Nordheim (FN) tunneling through the thin AlN barrier dominates.

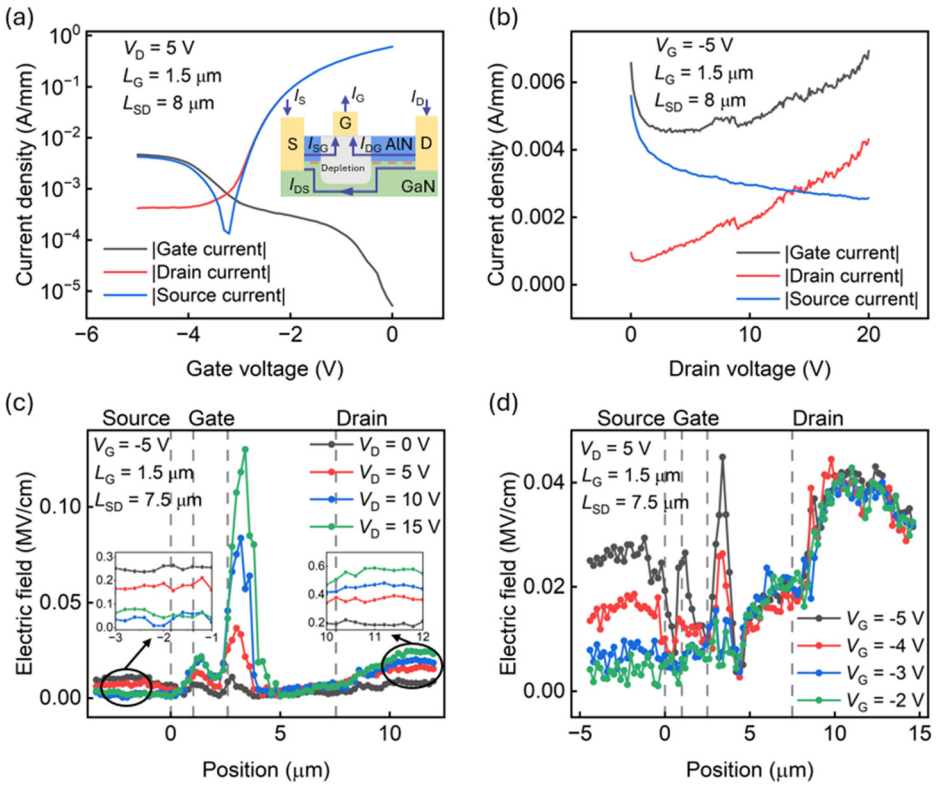

FIG. 3. (a) Three-terminal DC *IV* transfer characteristics of the AlN/GaN/AlN HEMT with 1.5 μm L_G and 8 μm L_{SD}. Inset: Schematic of the potential OFF-state leakage paths. (b) OFF-state leakage current vs drain bias. I_G has the opposite sign from I_D and I_S, and the absolute value of I_G equals the sum of I_D and I_S. (c) OFF-state electric field distributions from source to drain in the device with 1.5 μm L_G and 7.5 μm L_{SD} under different drain biases. α value of 1.5×10^{-3} is used to show the quantitative value of the lateral field between the source and the drain. The insets show the quantitative vertical fields beneath the source and the drain with α value of 3.5×10^{-2}. (d) Electric field distributions with different gate biases.

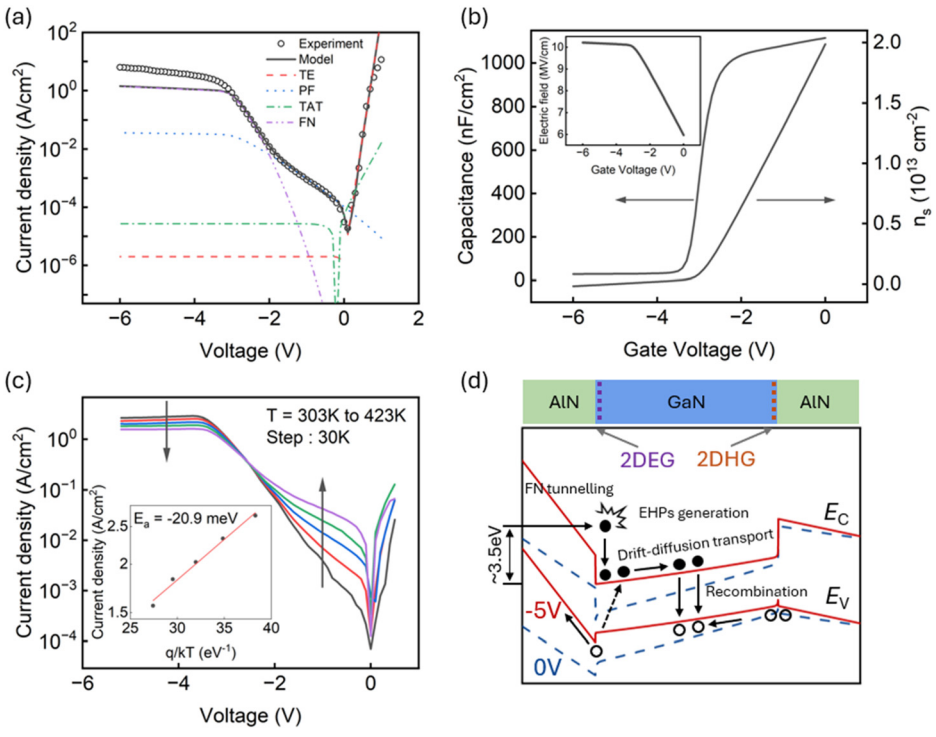

FIG. 4. (a) Gate leakage current of AlN/GaN/AlN HEMTs with 2 μm L_G and 5 μm L_{SD} as a function of gate bias modeled by different leakage mechanisms at different voltage ranges. The source contact is grounded, while the drain is floating. (b) CV characterization on a large area Schottky diode showing extracted 2DEG density and estimated electric field (supplementary material Note S2) across the barrier layer. (c) Temperature-dependent gate leakage current. Inset: Arrhenius plot of gate leakage current at −5 V. (d) Schematic band diagram under the gate at 0 and −5 V gate voltage and the schematic of the leakage process.

The model aligns well with the measured gate current until 2DEG depletion, beyond which the gate current surpasses the FN prediction. Notably, a strong negative temperature dependence [Fig. 4(c)] appears for $V_G > -3.5$ V, indicating an additional leakage process dominated by electron–hole pairs (EHPs) generation. This behavior is consistent with observations in AlGaN/GaN HEMTs with higher Al mole fractions, where FN tunneling governs leakage near threshold voltage.[29]

As illustrated in Fig. 4(d), electrons tunnel from the gate metal Fermi level through the AlN barrier via FN tunneling. Upon entering the GaN channel, these electrons possess a kinetic energy corresponding to the potential drop across the barrier and the gate threshold voltage ($\sim qV_{th}$).[30] This energy (~3.5 eV) is high enough to allow electrons to relax by generating EHPs. The secondary holes drift back to the gate, directly contributing to leakage. In the OFF state ($V_G < V_{th}$), the vertical band alignment between the depleted 2DEG region and the buried 2DHG resembles a forward-biased diode. Both the primary injected electrons and the secondary electrons created by EHPs generation transport vertically through the GaN channel via drift–diffusion and eventually recombine with holes supplied by the 2DHG.[31] This behavior is consistent with previous observations in AlN/GaN/AlN heterostructures, where recombination occurs between 2DEG and 2DHG.[6] To maintain charge balance and current continuity, the floating 2DHG potential shifts to a more negative value. This potential redistribution establishes a vertical electric field beneath the grounded ohmic contacts [as observed in Fig. 3(c)], which activates the PF-assisted vertical paths connecting the 2DHG to the source/drain. The coincidence between the gate-bias threshold for EHPs generation [Fig. 4(c)] and the onset of the vertical field beneath the source [Fig. 3(d)] confirms the correlation between EHPs generation and the activation of the 2DHG-mediated and PF-assisted leakage path. At higher temperatures, increased phonon scattering causes more tunneled electrons to lose energy before triggering EHPs generation. This suppresses the EHPs generation rate, leading to the observed reduction in overall gate leakage current [Fig. 4(c)].

Figure 5 summarizes these mechanisms using an equivalent circuit. In the OFF state ($V_G < V_{th}$), the electron injection from the gate via FN tunneling and subsequent carrier multiplication by EHPs generation act as the primary current source. The negative gate bias also forward-biases the effective diode between the depleted 2DEG and the buried 2DHG [Fig. 4(d)], enabling vertical carrier transport beneath the gate. This drives the floating 2DHG to a sufficiently negative potential to maintain charge balance. Consequently, a reverse-biased diode forms between 2DHG and n^{++} GaN beneath the source and drain contacts, establishing vertical electric fields at these terminals [Fig. 3(c)]. The 2DHG is then resistively connected to the ohmic contacts via a PF-assisted vertical leakage path [Fig. 2(f)]. Crucially, the continuous supply of carriers from the gate maintains the negative potential of the 2DHG and thus sustains the vertical field required for PF emission. The combination of gate injection, EHP-mediated potential regulation, and PF-assisted vertical path forms a parallel 2DHG conduction pathway, as indicated in Fig. 5. When a positive drain bias is applied, the vertical field under the source is screened while those beneath the gate and drain are enhanced [Fig. 3(c)], redistributing the leakage currents. Specifically, a V_{DS} of 2.5 V causes a 35% drop in I_{SG}, and 20 V V_{DS} causes a 55% drop in I_S [Fig. 3(b)]. Such a strong modulation would not occur if the leakage were dominated by surface paths, confirming that this 2DHG-mediated path is a primary component of the total leakage current.

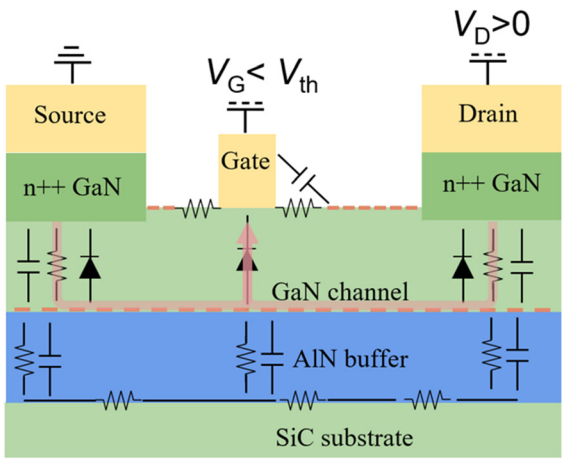

FIG. 5. Schematic of the equivalent circuit for the AlN/GaN/AlN HEMTs, showing the 2DHG leakage path.

The observed leakage paths and field redistribution provide direct evidence that the buried 2DHG forms a parallel conduction path in AlN/GaN/AlN HEMTs. Although the 2DEG dominates the on-state transport, the 2DHG contributes significantly to OFF-state leakage, reducing efficiency and degrading reliability. These findings motivate design strategies to suppress parasitic 2DHG conduction, such as employing high-k gate dielectrics[32] to suppress gate injection, introducing compensating n-type δ-doping to suppress 2DHG,[8,33] and using native AlN substrates[34] to minimize vertical conduction by reducing dislocation-related traps.

In summary, by combining electrical measurements with EFISHG field mapping, we identified distance-independent leakage and diode-like field distributions in AlN/GaN/AlN HEMTs, collectively demonstrating a parallel 2DHG-mediated leakage path. The leakage is governed by Fowler–Nordheim tunneling with electron–hole pairs generation and Poole–Frenkel vertical transport. These findings reveal the implications of parallel 2DHG conduction for device performance and establish EFISHG as a powerful tool to visualize hidden leakage paths.

See the supplementary material for the vertical leakage mechanism of the isolation structure (Note S1) and the gate leakage mechanism in AlN/GaN/AlN HEMTs (Note S2).

This work was supported as part of ULTRA, an Energy Frontier Research Center funded by the U.S. Department of Energy (DOE), Office of Science, Basic Energy Sciences (BES), under Award No. DE-SC0021230, and by the Engineering and Physical Sciences Research Council (EPSRC) under Grant No. EP/V057626/1.

AUTHOR DECLARATIONS

Conflict of Interest

The authors have no conflicts to disclose.

Author Contributions

Yuke Cao: Conceptualization (equal); Data curation (lead); Formal analysis (lead); Investigation (lead); Methodology (lead); Project administration (lead); Validation (lead); Visualization (lead); Writing – original draft (lead); Writing – review & editing (equal). **James W. Pomeroy:** Conceptualization (equal); Funding acquisition (equal); Investigation (equal); Supervision (equal); Validation (equal); Writing – review & editing (equal). **Austin Hickman:** Conceptualization (equal); Resources (equal). **Reet Chaudhuri:** Conceptualization (equal); Resources (equal). **Debdeep Jena:** Conceptualization (equal); Funding acquisition (equal); Resources (equal). **Huili Grace Xing:** Conceptualization (equal); Formal analysis (equal); Funding acquisition (equal); Methodology (equal); Resources (equal); Validation (equal); Writing – review & editing (equal). **Martin Kuball:** Conceptualization (equal); Funding acquisition (equal); Investigation (equal); Supervision (equal); Validation (equal); Writing – review & editing (equal).

DATA AVAILABILITY

The data that support the findings of this study are available from the corresponding author upon reasonable request.

REFERENCES

[1]Y.-K. Chen, T.-H. Chang, and A. Sivananthan, "Advanced mm-wave power electronics (invited talk)," in *IEEE BiCMOS and Compound Semiconductor Integrated Circuits and Technology Symposium (BCICTS)* (IEEE, 2019), pp. 1–4.

[2]G. Li, R. Wang, J. Guo, J. Verma, Z. Hu, Y. Yue, F. Faria, Y. Cao, M. Kelly, T. Kosel, H. Xing, and D. Jena, "Ultrathin body GaN-on-insulator quantum well FETs with regrown Ohmic contacts," IEEE Electron Device Lett. **33**(5), 661–663 (2012).

[3]A. Hickman, R. Chaudhuri, S. J. Bader, K. Nomoto, K. Lee, H. G. Xing, and D. Jena, "High breakdown voltage in RF AlN/GaN/AlN quantum well HEMTs," IEEE Electron Device Lett. **40**(8), 1293–1296 (2019).

[4]R. Chaudhuri, S. J. Bader, Z. Chen, D. A. Muller, H. G. Xing, and D. Jena, "A polarization-induced 2D hole gas in undoped gallium nitride quantum wells," Science **365**(6460), 1454–1457 (2019).

[5]S. J. Bader, H. Lee, R. Chaudhuri, S. Huang, A. Hickman, A. Molnar, H. G. Xing, D. Jena, H. W. Then, and N. Chowdhury, "Prospects for wide bandgap and ultrawide bandgap CMOS devices," IEEE Trans. Electron Devices **67**(10), 4010–4020 (2020).

[6]R. Chaudhuri, *Integrated Electronics on Aluminum Nitride: Materials and Devices* (Springer Nature, 2022).

[7]Y.-H. Chen, J. Encomendero, C. Savant, V. Protasenko, H. G. Xing, and D. Jena, "Electron mobility enhancement by electric field engineering of AlN/GaN/AlN quantum-well HEMTs on single-crystal AlN substrates," Appl. Phys. Lett. **124**(15), 152111 (2024).

[8]Y.-H. Chen, J. Encomendero, C. Savant, V. Protasenko, H. G. Xing, and D. Jena, "High conductivity coherently strained quantum well XHEMT heterostructures on AlN substrates with delta doping," Appl. Phys. Lett. **125**(14), 142110 (2024).

[9]C. Beckmann, J. Wieben, T. Zweipfennig, A. Kirchbrücher, J. Ehrler, R. Stamm, Z. Yang, H. Kalisch, and A. Vescan, "MOVPE-grown GaN/AlGaN heterostructures on sapphire with polarization-induced two-dimensional hole gases," J. Phys. D **55**(43), 435102 (2022).

[10]G. Zhan, F. Rampazzo, C. De Santi, M. Fornasier, G. Meneghesso, M. Meneghini, H. Blanck, J. Grünenpütt, D. Sommer, D. Y. Chen, K.-H. Wen, J.-T. Chen, and E. Zanoni, "Transconductance overshoot, a new trap-related effect in AlGaN/GaN HEMTs," IEEE Trans. Electron Devices **70**(6), 3005–3010 (2023).

[11]R. Chaudhuri, A. Hickman, J. Singhal, J. Casamento, H. G. Xing, and D. Jena, "In situ crystalline AlN passivation for reduced RF dispersion in strained-channel AlN/GaN/AlN high-electron-mobility transistors," Phys. Status Solidi A **219**(4), 2100452 (2022).

[12]A. Hickman, R. Chaudhuri, L. Li, K. Nomoto, S. J. Bader, J. C. Hwang, H. G. Xing, and D. Jena, "First RF power operation of AlN/GaN/AlN HEMTs with> 3 A/mm and 3 W/mm at 10 GHz," IEEE J. Electron Devices Soc. **9**, 121–124 (2021).

[13]Y. Cao, J. W. Pomeroy, M. J. Uren, F. Yang, and M. Kuball, "Electric field mapping of wide-bandgap semiconductor devices at a submicrometre resolution," Nat. Electron. **4**(7), 478–485 (2021).

[14]Y. Cao, J. W. Pomeroy, M. J. Uren, F. Yang, J. Wang, P. Fay, and M. Kuball, "Edge termination in vertical GaN diodes: Electric field distribution probed by second harmonic generation," Appl. Phys. Lett. **120**(24), 242106 (2022).

[15]Y. Cao, J. W. Pomeroy, and M. Kuball, "Characterizing electric fields in semiconductor devices: Effect of second-harmonic light interference," Opt. Lett. **49**(14), 4034–4037 (2024).

[16]W. Cai, A. P. Vasudev, and M. L. Brongersma, "Electrically controlled nonlinear generation of light with plasmonics," Science **333**(6050), 1720–1723 (2011).

[17]Y. Cao, "Electric field mapping in GaN based wide-bandgap semiconductor devices," Ph.D. thesis (University of Bristol, 2023).

[18]B. Rackauskas, M. J. Uren, S. Stoffels, M. Zhao, S. Decoutere, and M. Kuball, "Determination of the self-compensation ratio of carbon in AlGaN for HEMTs," IEEE Trans. Electron Devices **65**(5), 1838–1842 (2018).

[19]F. Abdollahi-Mamoudan, S. Savard, C. Ibarra-Castanedo, T. Filleter, and X. Maldague, "Influence of different design parameters on a coplanar capacitive sensor performance," NDT E Int. **126**, 102588 (2022).

[20]M. J. Uren, S. Karboyan, I. Chatterjee, A. Pooth, P. Moens, A. Banerjee, and M. Kuball, "Leaky dielectric' model for the suppression of dynamic R_{ON} in carbon-doped AlGaN/GaN HEMTs," IEEE Trans. Electron Devices **64**(7), 2826–2834 (2017).

[21]M. Cho, Z. Xu, M. Bakhtiary-Noodeh, T. Detchprohm, M. A. Daeumer, J.-H. Yoo, Q. Shao, T. A. Laurence, D. Key, and T. Hashimoto, "1.2-kV vertical GaN PIN rectifier with ion-implanted floating guard rings," IEEE Trans. Electron Devices **70**(9), 4578–4583 (2023).

[22]A. Pérez-Tomás, A. Fontserè, J. Llobet, M. Placidi, S. Rennesson, N. Baron, S. Chenot, J. C. Moreno, and Y. Cordier, "Analysis of the AlGaN/GaN vertical bulk current on Si, sapphire, and free-standing GaN substrates," J. Appl. Phys. **113**(17), 174501 (2013).

[23]L. Heuken, M. Alshahed, A. Ottaviani, M. Alomari, M. Heuken, C. Wächter, T. Bergunde, I. Cora, L. Tóth, B. Pécz, and J. N. Burghartz, "Temperature dependent vertical conduction of GaN HEMT structures on silicon and bulk GaN substrates," Phys. Status Solidi A **216**, 1800482 (2018).

[24]D. Cornigli, S. Reggiani, E. Gnani, A. Gnudi, G. Baccarani, P. Moens, P. Vanmeerbeek, A. Banerjee, and G. Meneghesso, "Numerical investigation of the lateral and vertical leakage currents and breakdown regimes in GaN-on-silicon vertical structures," in *IEEE International Electron Devices Meeting (IEDM)* (IEEE, 2015), p. 5.3.

[25]C. F. C. Chang, J. E. Dill, Z. Zhang, J.-C. Chen, N. Pieczulewski, S. J. Bader, O. A. Valenzuela, S. A. Crooker, F. F. Balakirev, R. D. McDonald, J. Encomendero, D. A. Muller, F. Giustino, D. Jena, and H. G. Xing, "Quantum oscillations of holes in GaN," arXiv:2501.16213 (2025).

[26]N. Faleev and I. Levin, "Strain and crystal defects in thin AlN/GaN structures on (0001) SiC," J. Appl. Phys. **107**(11), 113529 (2010).

[27]S. L. Zhao, B. Hou, W. W. Chen, M. H. Mi, J. X. Zheng, J. C. Zhang, X. H. Ma, and Y. Hao, "Analysis of the breakdown characterization method in GaN-based HEMTs," IEEE Trans. Power Electron. **31**(2), 1517–1527 (2016).

[28]S. Turuvekere, N. Karumuri, A. A. Rahman, A. Bhattacharya, A. DasGupta, and N. DasGupta, "Gate leakage mechanisms in AlGaN/GaN and AlInN/GaN HEMTs: Comparison and modeling," IEEE Trans. Electron Devices **60**(10), 3157–3165 (2013).

[29]S. Turuvekere, A. DasGupta, and N. DasGupta, "Effect of barrier layer thickness on gate leakage current in AlGaN/GaN HEMTs," IEEE Trans. Electron Devices **62**(10), 3449–3452 (2015).

[30]S. Turuvekere, D. S. Rawal, A. DasGupta, and N. DasGupta, "Evidence of Fowler–Nordheim tunneling in gate leakage current of AlGaN/GaN HEMTs at room temperature," IEEE Trans. Electron Devices **61**(12), 4291–4294 (2014).

[31]T. Tak, W. Y. Ho, I. Celupica-Liu, Y. C. Chow, J. Peretti, C. Weisbuch, and J. S. Speck, "Trap-assisted Auger-Meitner recombination in GaN p-i-n diodes," Phys. Rev. B **111**(15), 155308 (2025).
[32]A. Rawat, V. K. Surana, M. Meer, N. Bhardwaj, S. Ganguly, and D. Saha, "Gate current reduction and improved DC/RF characteristics in GaN-based MOS-HEMTs using thermally grown TiO_2 as a dielectric," IEEE Trans. Electron Devices **66**(6), 2557–2562 (2019).
[33]E. Kim, Y.-H. Chen, K. Shinohara, T.-S. Nguyen, J. Encomendero, D. Jena, and H. G. Xing, "4.2 W/mm at 10 GHz in silicon delta-doped AlN/GaN/AlN pseudomorphic HEMTs with PECVD SiN passivation," IEEE Electron Device Lett. **46**(10), 1729–1732 (2025).
[34]E. Kim, Z. Zhang, J. Encomendero, J. Singhal, K. Nomoto, A. Hickman, C. Wang, P. Fay, M. Toita, and D. Jena, "N-polar GaN/AlGaN/AlN high electron mobility transistors on single-crystal bulk AlN substrates," Appl. Phys. Lett. **122**(9), 092104 (2023).